

Aptamer-Modified Nanohydrogel Microarrays for Bioselective Cancer Cell Immobilization

Zan Lamberger, Hendrik Bargel, and Martin Humenik*

Photolithography combined with surface nucleated protein self-assembly of azido-modified spider silk proteins is used to create an arbitrarily shaped, inherently cell repellent micropattern based on nanofibrillar networks. Using “click” chemistry with dibenzocyclooctin modified oligonucleotides, the microstructures are functionalized with DNA-aptamers, which selectively bind cancer cell markers protein tyrosine kinase 7 or nucleolin. The epitope-specific cell interaction on the aptamer-modified surfaces is tested using human non-adherent leukemia T cells (Jurkat), as well as adherent cervix carcinoma (HeLa) and neuroblastoma (Kelly) cells. The cells can be immobilized with high precision and cell densities on the pattern, also revealing spatially defined proliferation and spreading into distinct morphologies upon cultivation. The formation of integrin-based focal adhesions occurs in the case of the aptamer immobilized cancer cells, similarly to those anchored on RGD-modified pattern. The firm aptamer-marker anchorage allows for the formation of integrin-dependent cell adhesions. Due to the amenability of the recombinant spider silk protein towards chemical and genetical modifications, the presented micropatterned fibrous networks have great potential for further development of adjustable and biocompatible cell-specific arrays, enabling applications in circulating cancer cell isolation and cultivation, studies on the cell's pathogenesis, progression and metastasis capabilities as well as enabling development of platforms for personalized medicine.

1. Introduction

Cancer cell research and therapy remain one of the frontiers of biomedical research and development, despite many advances in the last decades. Early detection of tumors is still

challenging, since these are often discovered unintentionally as part of an undergone medical procedure or, in later states, due to associated problems with the resident tissue.^[1] Contrarily, a quick identification and treatment of a tumor is crucial for successful healing as well as for prevention of its recurrence. Hence, rapid detection and analysis of the cancer cells became an essential prerequisite for improved therapies.^[2]

There are several ways to obtain cancerous cells from a patient, the most common being tissue biopsies where tumor segments are removed surgically. Depending on the location of the tumor, such procedures can be difficult and very invasive for the patient. In comparison, liquid biopsies present a less invasive approach, since the bodily fluids can be analyzed for cancer cells.^[3] The analysis of blood samples for circulating tumor cells (CTCs), which have detached from the main site of growth,^[4] has been established as a convenient patient-friendly method.^[5] The concentration and phenotype of the cells could be used to elucidate the state


of the tumor and the associated progression of the disease, as well as monitor the success of any administered treatment.^[6] Moreover, it is advantageous if separated cells remain in a viable state for later culturing and cell analyses. Specifically, the isolation of cancer cells and close monitoring of the cancer progression becomes essential for specific drug targeting and therapeutic successes, decreasing the risk of relapse.^[7]

Many cancer cell targeting methods focus on markers,^[8,9] represented by membrane proteins which are specifically overexpressed,^[9] altered^[10], or even relocated into the outer membrane^[11] due to malignant cell transformations. Typical examples are protein tyrosine kinase 7 (PTK7), a plasma membrane protein,^[12] as well as nucleolin, which is relocated from the nucleus to the outer cell membrane during oncogenesis.^[13,14] The same inherent epitopes could also be exploited for specific cancer cell targeting and isolation using immobilized antibodies or aptamers.^[15]

Adequate surfaces for such type of cell immobilization are required to be non-adhesive for proteins and cells,^[13,16] non-toxic and easily modifiable to enable strong, specific, and tunable marker binding.^[17] Recombinant spider silk proteins present a biocompatible material,^[18] which can be processed into cross-beta nanofibrils under mild aqueous conditions. The

Z. Lamberger, H. Bargel, M. Humenik
Department of Biomaterials
Faculty of Engineering Science
Universität Bayreuth
Prof. Rüdiger-Bormann, Str. 1, 95447 Bayreuth, Germany
E-mail: martin.humenik@bm.uni-bayreuth.de

Z. Lamberger
Department of Functional Materials in Medicine and Dentistry
University of Würzburg
Pleicherwall 2, 97070 Würzburg, Germany

 The ORCID identification number(s) for the author(s) of this article can be found under <https://doi.org/10.1002/adfm.202207270>.

© 2022 The Authors. Advanced Functional Materials published by Wiley-VCH GmbH. This is an open access article under the terms of the Creative Commons Attribution License, which permits use, distribution and reproduction in any medium, provided the original work is properly cited.

DOI: 10.1002/adfm.202207270

nucleated self-assembly is triggered by a low concentration of phosphate ions in solutions.^[19,20] Employing surfaces of the same protein containing beta-sheet rich structures, e.g., microparticles,^[19] molecular monolayers^[21] or nanofilms,^[22] the fibril formation could be re-directed onto these surfaces, resulting in immobilized fibrous networks with nanohydrogel properties.^[22] The nanohydrogels showed inherently non-adhesive surface properties for cell and protein binding, whilst at the same time enabling incorporation of diverse DNA functionalities and related addressable immobilization of enzymes or DNA-modified cells.^[22,23] Moreover, the chemical resilience of the fibrous networks enabled photolithography procedures and the production of nanohydrogel micropattern.^[23]

Herein we used the photolithographic approach to create arbitrarily shaped microwells to spatially define the self-assembly of azido-modified recombinant spider silk protein N₃-eADF4(C16) into microstructured networks on surfaces. Modification of the protein pattern via copper-free strain-promoted cycloaddition enabled incorporation of DNA-aptamers to bind typical cancer markers PTK7 or nucleolin expressed on human non-adherent leukemia T cells (Jurkat), as well as adherent cervix carcinoma (HeLa) and neuroblastoma (Kelly) cell lines. The aptamer-marker interaction was studied in the cell suspensions as well as on spatially constrained surface microstructures made of the aptamer-modified spider silk fibrils.

2. Results and Discussion

2.1. Aptamer Binding Affinity in Cell Suspensions

The expression of cancer marker PTK7 and/or nucleolin depends on cultivation conditions and the developmental stadium of the cells. The re-localization of nucleolin into the cell membrane has been reported for HeLa and Jurkat cells^[14,24] and proposed for the Kelly line.^[25] The overexpression of PTK7 in the case of Jurkat,^[26,27] HeLa,^[28] and Kelly^[29] lines has been shown as well. To test which of the typical markers is presented in the cell membranes under the employed cultivation conditions, we analyzed the binding of fluorescently labeled tetramethylrhodamine (TAMRA)-DNA aptamers sgc8 (anti-PTK7)^[26] and AS1411 (anti-nucleolin)^[30] to the cell surface using flow cytometry. Moreover, we also determined the difference between the 3'- or 5'-modified aptamer variants in their marker affinity (Figure 1A, B and Figure S1, Supporting Information). In general, both aptamers, the anti-PTK and the anti-nucleolin possessing 5'-TAMRA revealed a clear affinity to Jurkat and HeLa cells, as well as weaker binding to Kelly cells. In comparison, weaker bindings were observed in case of the 3'-modified aptamers to the Jurkat and HeLa cells and no binding to the Kelly line. Thus, for further functionalization of spider silk fibrous networks and for cell-surface immobilization studies 5'-modified aptamers were employed herein.

2.2. Marker-Based Cell Immobilization on Fibrous Nanohydrogels

The recently established preparation of eADF4(C16) nanohydrogels immobilized on surfaces^[22,23] was used to assemble

N₃-eADF4(C16) in well-plates coated by the unmodified protein. Hence, the self-assembled nanohydrogels could be functionalized using 5'-dibenzocyclooctin (DBCO) oligonucleotides. We optimized the system to increase the DNA functionalization capacity of the nanohydrogels. First, the amount of the protein in the film employed to nucleate the fibril assembly was compared with amount of the self-assembled material on top. Therefore, eADF4(C16) was coupled with carboxy fluorescein (cFlu) on its N-terminus.^[19] Films cast in well plates revealed a twice as high fluorescence signal in comparison to the same protein assembled in the nanohydrogels on top (Figure S2A, Supporting Information). In the next step, we optimized the azide-alkyne coupling reaction, testing different reaction times and temperatures, since the catalyst-free strain-promoted cycloaddition reveals typically lower reaction rates,^[31] requiring 3 days for the efficient coupling of nucleic acids to the spider silk networks.^[23] As the spider silk fibrils represent a robust nanomaterial withstanding even higher temperatures,^[32] reaction conditions up to 80 °C were tested. The amount of oligonucleotide coupled on to the nanohydrogel substrates was examined using a complementary fluorescein amidite (FAM) modified probe (Figure S2B, Supporting Information). The reaction at 80 °C resulted in a doubled coupling yield in one

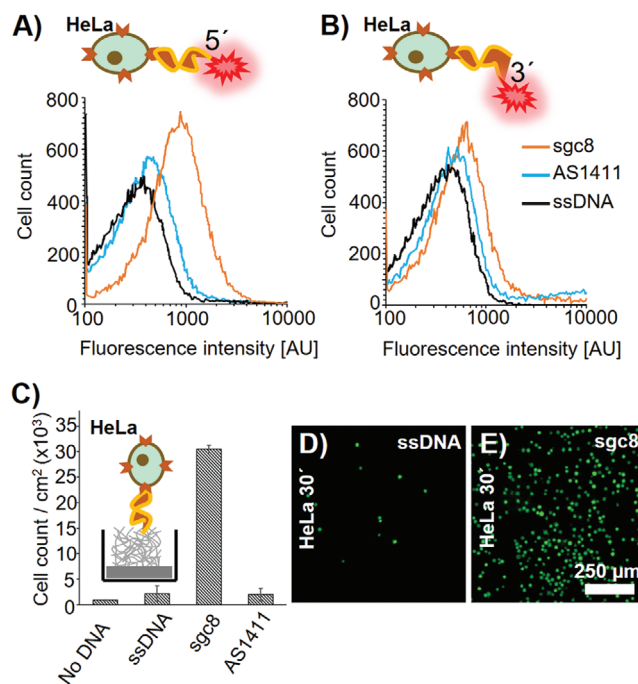


Figure 1. Analysis of aptamer-cell binding in solution and on aptamer-modified nanohydrogels. The binding of TAMRA modified aptamers sgc8 (orange), AS1411 (blue) and the ssDNA control (black) was tested on HeLa cells in case of the 5'- (A) and 3'- modification (B) in solution. Further, HeLa cells were seeded on unmodified, ssDNA, and correspondingly aptamer-modified nanohydrogels for 30 min and counted after the washing steps in (C) showing specific binding to the anti-PTK aptamer on the surface. To demonstrate the differences in specific and unspecific cell binding, fluorescence microscopic images showing the distribution of the cells on ssDNA and sgc8 modified surfaces are shown in (D) and (E), respectively. Plotted values in (C) presented as mean \pm cell counts, $n = 3$, p -values were calculated using a one-way ANOVA, $*p < 0.05$. Scale bars in (D) and (E) 250 μm .

third of the reaction time compared to the previously used 37 °C^[23] (Figure S2B, Supporting Information). The nucleic acid coupling capacities of both the film and the nanohydrogel morphologies were compared as well (Figure S2C Supporting Information). Considering a two times higher amount of protein in the film as in the nanohydrogel (Figure S2A, Supporting Information), the normalized binding capacity of the oligonucleotides in nanohydrogel was sixteen times higher than on the film.

Using the optimized setup in well-plates, the N₃-modified nanohydrogels were further functionalized with 5'-DBCO-sgc8 or -AS1411 aptamers. The binding preferences of cancer cell lines to the aptamers in suspension (Figure 1A, B, Figure S1, Supporting Information) were compared to the binding capability of aptamer-modified nanohydrogels (Figure 1C–E, Figure S3, Supporting Information). Densities of the immobilized cells on the tested surfaces (Figure 1C–E and Figure S3, Supporting Information) revealed that the anti-PTK aptamer was highly suited to anchor all the screened cancer cell lines. In comparison to the flow cytometric analysis, where the sgc8 was only weakly bound to the Kelly line (Figure S1C, D, Supporting Information), the immobilization efficiency on the nanohydrogel surface (Figure S3D, F, Supporting Information) was comparable to that of the Jurkat and HeLa lines. This could be explained by a probable multiple aptamer binding between the nanohydrogel and the cell surface resulting in a higher avidity in comparison to the corresponding affinity of individual aptamers,^[33] used in the flow cytometric analysis in solution. Current fluorescence activated (FACS) or magnetic activated (MACS) cell sorting systems^[34] rely on affinity-based one-to-one binding between the cellular marker and labeled antibody tracker, whereas avidity-based cumulative binding of aptamers to cancer cells immobilized on the nanohydrogels could represent an advantage in future developments of devices, providing more sensitive and specific isolation of rare (low-concentration) CTCs. Moreover, the presented surface platform made of the biocompatible protein-fibril scaffold can also directly serve as a culturing surface, eliminating the need for further downstream handling as in FACS and MACS, since the coupled recognition antibodies carrying fluorescent dyes and magnetic beads, respectively, could affect the subsequent cell culture via cytotoxic effects. Depending on their size and composition, magnetic nanoparticles can also be taken up by the cell and potentially lead to cell damage.^[35]

Importantly, the unmodified nanohydrogels and nanohydrogels modified with a random single-stranded DNA sequence (ssDNA) showed only negligible unspecific cell binding (Figure 1C and Figure S3, Supporting Information). Specificity of the aptamer-marker interaction was also tested. After immobilization of Jurkat cells on a sgc8 modified nanohydrogel surface, an aptamer complementary probe was added. Due to the formation of double-stranded DNA, the changed secondary structure of the aptamer resulted in resolving of the conformation dependent binding to the marker and release of the cells (Figure S4, Supporting Information).

To assess the aptamer-modified nanohydrogels concerning their cell binding capabilities, we compared HeLa binding to sgc8 aptamer in Figure 1C–E to surfaces made of eADF4(C16)-RGD variant (Figure S5, Supporting Information), which has

been established to enhance attachment of cells to spider silk-based coatings^[36,37] and printable hydrogels.^[38,39] On the one side, the aptamer-to-marker binding resulted in similar binding densities as native RGD-to-integrin binding on the corresponding protein films (both at $\approx 55\,000$ cells cm⁻²). On the other side, assembled nanohydrogels made of the same protein displayed approximately 40% better cell adhesion in comparison to the RGD-films (Figure S5, Supporting Information) likely due to improved binding motif accessibility. This supports our findings on increased density of the exposed binding sites enabled by the fibrillar nature of the nanohydrogels (Section 2.2, Figure S2, Supporting Information).

Despite detected weak binding of anti-nucleolin AS1411 to the cell lines studied in suspension (Figure 1A and Figure S1A, Supporting Information), negligible cell immobilization was observed on the correspondingly modified fibrous surfaces (Figure 1C and Figure S3A, Supporting Information). The secondary structure of the G-quadruplex aptamer AS1411 reveals polymorphism of antiparallel and parallel topologies which equilibrium enables binding of the proper conformations to the nucleolin ligand.^[11,40] However, such equilibrium is not present in case of the immobilized aptamers in the fibrous networks, thus most probably a reduced population of the proper conformations along with observed weak overexpression of the marker resulted in the lack of cell immobilization.

The affinities between the aptamers and the markers may differ significantly between suspension and surface targeting approaches, as shown here. In general, a higher affinity at the surface could be expected due to the enhanced interaction of the cell surface with the immobilized aptamers. However, the secondary structure of the aptamers, which is uniquely defined for the specific aptamer/marker pair, could lead to loss of binding due to surface-related constraints.

2.3. Spatially Controlled Cancer Cell Immobilization on Micropatterned Nanohydrogels

As shown in our previous research, the spider silk protein fibrous networks were sufficiently stable in photolithography procedures.^[23] A positive-tone photoresist was applied on amino-modified glass substrates to produce microchambers with an accessible chemically modified bottom (Figure S6A and B, Supporting Information), followed by the site-specific covalent immobilization of the recombinant silk protein and surface nucleated self-assembly of azido modified fibrous networks in the micropatterned reaction vessels. After removal of the photoresist, the fibrous pattern was modified using DBCO-oligonucleotides, similar to the nanohydrogels in the well format (Figure S6C, Supporting Information). Before application of the cells, the exposed amino surface was blocked using branched PEG, enhancing the cell repelling effect of the non-patterned areas.

To test the site-specific immobilization of cancer cells, the micropatterned surfaces were functionalized with anti-PTK aptamers and seeded with the Jurkat, HeLa and Kelly cell lines. Fluorescence images of the live stained cells (Figure 2) showed that all tested cell lines preferentially bound on the micropattern made of anti-PTK modified fibrous networks.

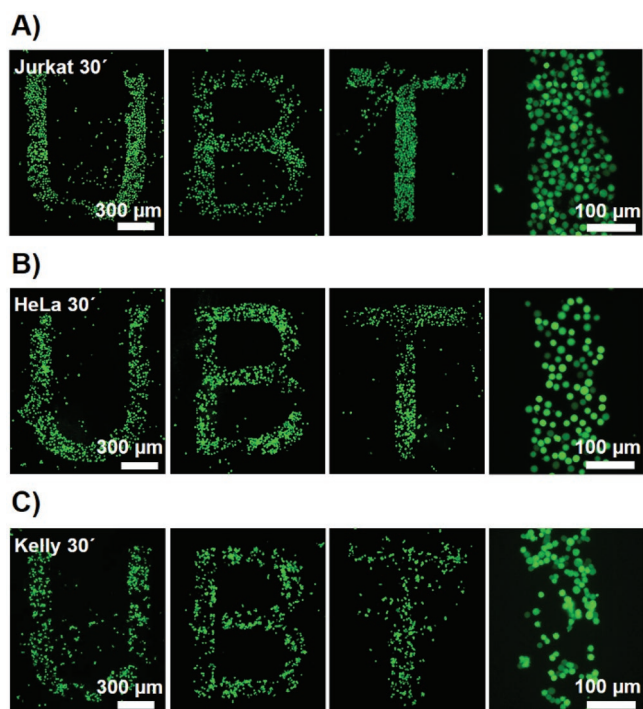


Figure 2. Immobilization of various cell lines on U-, B- and T-letter micropattern assembled from anti-PTK aptamer-modified fibrous networks. Fluorescence microscopic images of live stained Jurkat in (A), HeLa in (B) and Kelly cells in (C) at two different magnifications after a 30 min immobilization and subsequent washings. Scale bars for whole UBT pattern 300 μm in (A)–(C).

Outside of the pattern, the adherent Kelly and HeLa as well as non-adherent Jurkat cells showed a similar low affinity to the PEG-modified surface due to its high hydrophilicity.^[41] Since Kelly cells formed clusters during their cultivation and re-suspension, the aptamer-based immobilization of the cells in well plates (Figure S3E and F, Supporting Information) as well as on the patterned surface (Figure 2C) resulted in less homogeneous distributions compared to well resuspended HeLa (Figures 1 and 2B) or Jurkat cells (Figure S3B, Supporting Information and C, Figure 2B). Moreover, the clustered cells revealed higher avidity for the aptamer-modified surfaces than single cells from the mixture, hence being more resilient to washing-off. The spatial binding selectivity of the aptamer-modified pattern was compared to those made of unmodified protein or the protein-modified with ssDNA, showing only randomly deposited cells with very low coverage density (Figure S7, Supporting Information, shown exemplarily for HeLa).

2.4. Micropattern with Mixed Functionalities

An advantage of self-assembling three-dimensional fibrous networks is not only the high binding capacity, as demonstrated in Figure S2 (Supporting Information), but also the possibility to produce functionally mixed networks, as demonstrated on a macroscopic fibrous system with two different thrombin binding aptamers, recently.^[22] Here, the dual functionalization of the micropatterned system was demonstrated by combining

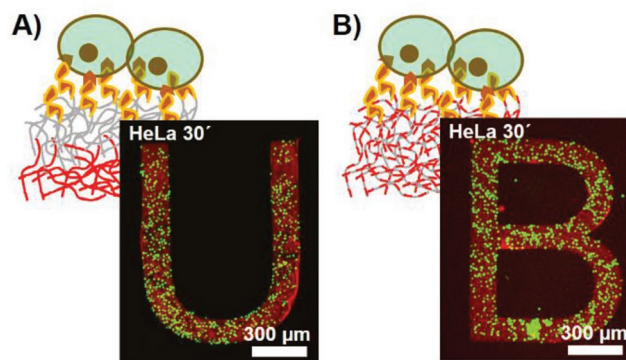


Figure 3. HeLa cells immobilized on double labeled micropattern. Nano-hydrogels of TAMRA-eADF4(C16) were assembled in the microwells either consecutively in (A) or in a mixture in (B) with N_3 -eADF4(C16). Finally, the mixed networks were activated for cell binding using coupling of DBCO-aptamers.

self-assembly of the functionable N_3 -eADF4(C16) and fluorescently labeled TAMRA-eADF4(C16), whereas the dye served as a model for a covalently coupled drug in the microstructured network of fibrils (Figure 3).

In the consecutive assembly and in the co-assembly approach (Figure 3A, B) respectively, HeLa cells could be immobilized in similar densities compared to the monofunctionalized pattern (Figure 2), whereas presence of the red fluorescent dye was clearly visualized resembling the shape of the micropattern. In future developments, such aptamer-modified networks could be combined for example with spider silk variants containing switchable linkers for triggered drug release^[42] which could be explored in combination with the aptamer-based cancer cell immobilization in parallel.

2.5. Switch in Cell Attachment Mechanism upon Cultivation on Fibrous Micropattern

We tested prolonged cultivation of the cells on the micropatterned substrates, along with investigating possible residual cytotoxic effects of the employed photolithography process. To produce cell attractive conditions as a positive control for the cultivation, we also prepared a fibrous pattern from an adhesion promoting eADF4(C16)-RGD. We compared the RGD-pattern allowing cell-unspecific, integrin-mediated binding (Figure 4A/1–D/1) to the specific PTK-aptamer interaction on microstructures using HeLa and Kelly cells, respectively (Figure 4A/2–D/2, A/3–D/3). Contrarily to the round-shaped cells visible directly after surface binding (Figure 2,3), the cultivated cells revealed apparent spreading (Figure 4B and Figure S8, Supporting Information) and covered up to 70% of the RGD modified pattern, while 30–40% was covered on the aptamer-modified variants (Figure S8B, Supporting Information). The HeLa cells immobilized on the aptamer-modified nanohydrogels (Figure 4A/2) spread slower than those on the RGD substrate (Figure 4A/1), reaching the full confluence on the micropattern after 24 h in comparison to 6 h, respectively. The spreading cells preferred to orient inside of the micropattern borders, which was well visible especially in case of the

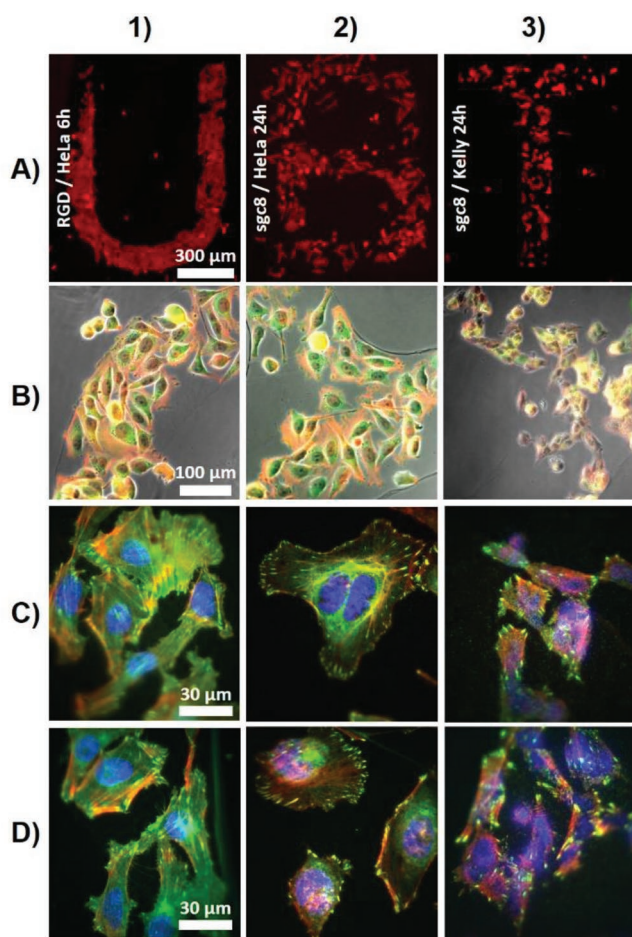


Figure 4. Spreading HeLa and Kelly cells on micropatterned protein networks. HeLa cells were immobilized and cultured on the RGD in (1) and anti-PTK aptamer modified pattern in (2), whereas Kelly cells were cultivated on the aptamer micropattern in (3). The cells were stained for vinculin in green, the actin cytoskeleton in red and nuclei in blue and visualized at different magnifications in (A)–(D) after 6 h in (1) and 24 h in (2) and (3) of cultivation. Fluorescence microscopy was used in (A) and (B), bright field in (B) and the colocalization of vinculin and actin in the membrane on the cell-substrate interface was depicted using TIRF microscopy in (C) and (D). Scale bars 300 μm in (A), 100 μm in (B) and in 30 μm (C) and (D).

highly confluent HeLa cells (Figure 4B/1,2), elongating along the edges and not expanding onto the pegylated surface. The cells which occasionally remained aside from the pattern after the seeding and washing steps, however, kept the initial round shape, hence highlighting the biocompatibility of the fibrous pattern (Figure S8A, Supporting Information). The differences between cells on distinctly modified surfaces as well as between the studied cell lines were investigated using focal adhesion staining. Total internal reflection fluorescence (TIRF) microscopy^[43] enabled focusing on the cell-membrane/nanohydrogel interface (Figure 4C,D). The fast cell spreading in case of the RGD surface modification, enabled due to native integrin-based adhesion, was accompanied by the formation of numerous focal points across the whole cell-to-substrate contact area (Figure 4C/1,D/1). The clusters resulted from overlay of the green fluorescence stained vinculin at the ends of red

fluorescence stained actin filaments.^[44] Interestingly, the focal adhesions could be observed also in case of spreading HeLa (Figure 4C/2,D/2) and Kelly cells (Figure 4C/3,D/3) after 24 h, despite the cells being initially immobilized via marker-aptamer interactions. In case of HeLa cells, the density of focal points across the membrane was apparently lower in comparison to the dense network on the RGD surface (compare C and D). In The 1st and 2nd rows in Figure 4), but overall the cells on both substrates revealed a similar number of focal adhesions, whereas the Kelly line (Figure 4C/3,D/3, Figure S8C, Supporting Information) formed rather rare focal props on the cell borders, most probably due to the cell's preference to form multicellular clusters instead of monolayers.

Research on cell adhesion motif independent immobilization suggests that firmly bound cells may exert mechanisms for cytoskeletal rearrangement resulting in spreading-like morphologies.^[45] However, the observed focal adhesions typically form upon integrin clustering processes around cell adhesive motifs, such as RGD, which facilitate cell attachment and spreading within the extracellular matrix (ECM).^[44,46] Cancer cells are prone to obtain their oncogenic behavior by altering innate cell adhesion and motility pathways. It is well-established that cancerous cells have a profound role in remodeling their surrounding by reorganization and degradation of pre-existing ECM architecture, or by stimulating local matrix secretion.^[47] Moreover, stabilization of cell-to-surfaces binding could initiate upregulation of ECM component secretion and focal adhesion formation.^[48] Although, the aptamer-spider silk networks lack native cell binding motifs, the firm aptamer-marker binding on nanohydrogels (C and D in the 2nd and 3rd rows in Figure 4) apparently provided sufficient time to start cellular remodeling of the proximate fibrous spider silk-based networks via incorporation of native ECM components, resulting in the successful cell proliferation. Previously, spider silk protein materials displayed good long-term biodegradability *in vitro* by enzymes^[49] and *in vivo*,^[50] rendering them well suited scaffolds for tissue engineering. The solid hydrogels of self-assembling silk proteins provided sufficient stability for the initial immobilization and cultivation phases and allowed the captured cells to gradually replace the artificial scaffold and create a native cell environment without negatively affecting cellular homeostasis.^[38,39,50] The stability of the aptamers involved is also apparently sufficient for both the cell immobilization, as they can still be detected after cell release by annealing a fluorescent probe (Figure S4C, Supporting Information) and the cultivation enabling cell spreading (Figure 4). In our previous study, cultivation of DNA-modified HeLa cells immobilized on complementary modified nanohydrogels failed due to short-term stability (<2 h) of the DNA modification integrated via a lipid anchor into the cellular membrane.^[23]

3. Conclusion

Recombinant spider silk protein was used as seeding surfaces upon which an azido-modified protein variant was self-assembled into fibril-based networks. The nanohydrogels were functionalized with anti-marker DNA-aptamers using “click” chemistry, thereby turning the otherwise cell

repellent spider silk nanohydrogels into scaffolds enabling the marker-dependent cancer cell immobilization. The established principles were applied to the formation of nanohydrogel micropattern via photolithography. The Jurkat, HeLa and Kelly cell lines could be immobilized by employing selective interaction between cellular marker PTK7 and aptamer sgc8 incorporated into the protein nanohydrogel. Unmodified microstructures or those modified with a random nucleic acid sequence remained cell repellent. However, the stable aptamer-based cancer cell binding provided the possibility of prolonged cell cultivation leading to cell spreading and confluency within the microstructures after 24 h. The investigation of a vinculin/actin colocalization on the cell membrane-surface interface using TIRF revealed the formation of integrin-related focal adhesions, similarly to those found on RGD-microstructures. The finding points toward cancer remodeling processes resulting in successful interpenetration of the fibrous spider silk matrix with secreted native ECM components.

The demonstrated patterning of the biocompatible recombinant spider silk RGD-tagged and aptamer conjugate variants combined with its genetic^[37,51] and chemical modification capability^[22,23,32,52] as well as variability of the applied photolithographic approach in relation to the pattern shapes and dimensions, confer the potential of the microstructured DNA-modified fibrous networks for the preparation of multifunctional and selective cell binding substrates. The genetical and chemical modifiability of the system represents a clear advantage in comparison to other commonly employed protein^[53] or polysaccharide-based platforms^[54] which are accessible only to chemical modifications. In addition, self-assembly of spider silk variants offers the possibility of co-assembly, allowing adjustment of the composition and concentration of exposed binding motifs.^[22] Compared to synthetic polymers, although characterized by their variability in producing microstructured systems for cell interactions,^[55] the proteinaceous and fibrillar nature of the spider silk system is more similar to native ECM, along with its biodegradability and remodeling capability.

Selective isolation and cultivation of tumor cells are of profound importance in the fields of medicine, pharmacology, and molecular biology. The presented compatibility of the micropatterned nanohydrogel surface with cancer cell culturing conditions is advantageous for designing of platforms which enable profiling and identification of immobilized cancer cells using visualization of distinct membrane markers.^[56] In further developments, the presented system of the micropatterned nanohydrogels can be joined with polydimethylsiloxane (PDMS)-based microfluidics to create CTC isolation devices. These could be used for further culturing and profiling of the cell samples to gain insights into cancer progression and metastasis based on the characteristics of the captured and subsequently cultured cells. In addition, it may be possible to transfer the 2D cell substrates after cell immobilization to a 3D environment that is more native to most cells by using higher concentration solutions of the spider silk proteins (>1% w/v) that readily self-assemble into fibril-based hydrogels.^[39] Such hydrogels, if applied on top of the micropatterned platform, would be useful to study proliferation, migration, and formation of multicellular cancer-based systems in ECM-like fibrous environments. Such properties of circulating tumor cells significantly influence

their role in metastasis.^[57] In addition, the arbitrarily changeable shape and composition of the micropattern could be used for studies on the influence of different shapes and topographies on cell differentiation and proliferation and/or in cell migration experiments.^[58] Thus, the presented development of microstructured aptamer-functionalized fibrous networks represents a crucial step in the generation of tunable cellular arrays enabling the culture of CTCs and valuable studies on their pathogenesis, progression and metastasis capabilities, especially with a focus on personalized medicine.

4. Experimental Section

Photolithographic Preparation of Patterned DNA-Modified Fibrous Networks: Glass coverslips (\varnothing 19 mm) were cleaned using acetone, isopropanol and the Radio Corporation of America (RCA) procedure, before activation with 100% O₂-plasma at 0.2 mbar for 1 min and a silanization using 0.1% (v/v) APTES in ethanol for 16 h, as described.^[59] The amino activated slides were pre-baked at 120 °C for 10 min on a precision hot plate HP 60 (Präzitherm PZ 28-2, Harry Gestigkeit GmbH, Germany) to evaporate adsorbed H₂O. Afterward, the coverslips were placed onto a spin coater SCE-150 and 55 μ l of Ti-Prime (Microchemicals GmbH, Germany) were applied at 50 rps for 30 s with an acceleration time of 3 s. The coated plates were incubated for 2 min at 120 °C on the hotplate and spin coated with 55 μ l of the Microposit 1813 G2 positive photoresist (Micro Resist Technology, Germany) followed by spin coating of 55 μ l of the AZ 1512 HS positive photoresist (Microchemicals GmbH, Germany) resulting in a combined photoresist thickness of approximately 1 μ m. The coverslips were post-baked at 115 °C for 1 min, and subsequently illuminated using a mask-less lithography equipment SmartPrint based on a μ LCD projection technology (Microlight3D) at 435 nm (10.2 mW cm⁻²) for 60 s. The microwells were developed in 1:4 (v/v) AZ 400 K Developer (Microchemicals GmbH, Germany)/H₂O solution using agitation for 30 s. To render the microstructures more resilient against longer incubations in aqueous media, hardening was conducted using exposure to a deep UV light (Benda NU-6 KL UV lamp) at 254 nm for 2.5 min.

After the photolithography, the amino-modified surfaces in the deprotected micro wells were covalently modified in a solution of 2.5 μ M eADF4(C16) and 2.5 mg/ml *N*-(3-dimethylaminopropyl)-*N'*-ethylcarbodiimid (EDC) hydrochlorid in 50 mM HEPES-Na, pH 7.1 for 16 h. Thereafter the coverslips were washed with 50 mM HEPES-Na pH 7.1 and incubated in a solution of 5 μ M N₃-eADF4(C16) or the fluorescently modified variant in 100 mM K-Pi, 50 mM HEPES pH 7.1 for 16 h, similarly to the preparation of the nanohydrogel in well-plates (see Supporting Information). K-Pi buffer was used to initiate the self-assembly of fibrils.^[19] The coverslips were washed with 10 mM Tris/HCl 100 mM NaCl and Milli-Q H₂O.

The photoresist was stripped using a bright field lamp (Makita DEADML801) at the maximum intensity for 2 min followed by 10 min incubations in solutions of 1:4 (v/v) AZ 400 K Developer/H₂O, 2:1 (v/v) acetone/ethyl acetate, acetone and Milli-Q H₂O.

After the stripping procedure, N₃-eADF4(C16) nanohydrogel micropattern was covered with 50 μ l of 5 μ M DBCO-DNA in 10 mM Tris/HCl 100 mM NaCl pH 7.5 at 80 °C for 24 h in a humid atmosphere. The coverslips were washed with 10 mM Tris/HCl 100 mM NaCl pH 7.5 and H₂O, followed by drying with compressed air.

Finally, the deprotected APTES modified glass surface with the nanohydrogel pattern, was blocked using 5 μ M *N*-hydroxysuccinimide activated TMS(PEG)₁₂ (Thermo Scientific Pierce) in 50 mM HEPES pH 7.1 for 16 h. Afterward, the coverslips were washed with 10 mM Tris/HCl 100 mM NaCl and H₂O, followed by air drying and storage at 4 °C.

Cell Capture on Microarrays: The patterned substrates were sterilized with 70% ethanol for 10 min and washed thrice with Aptamer buffer (10 mM Tris/HCl pH 7.5 100 mM NaCl, 25 mM KCl, 5 mM MgCl₂).

The passaged cells stained with 0.3 μM Calcein AM (live staining) were seeded onto the coverslips (350 000 cells cm^{-2} for the immobilization and 100 000 cells cm^{-2} for the immobilization with subsequent cultivation). The suspension was left to sediment for 30 min at RT and the coverslips were washed 3–5 times with PBS, to remove unbound cells. The remaining cells were visualized with a fluorescence microscope (DMI8, Leica Microsystems GmbH, Germany).

Focal Adhesion Immunostaining: The Actin Cytoskeleton and Focal Adhesions Staining Kit (EMD Millipore Corp., USA) with a modified protocol was used for the staining. The medium was withdrawn from the wells, and 3.7% (v/v) Glutaraldehyde in PBS (115 mM NaCl, 4 mM KH_2PO_4 , 16 mM Na_2HPO_4 , pH 6.8) was applied onto the cells and incubated for 20 min, followed by two wash steps with PBS containing 0.05% (v/v) Tween-20 and permeabilization with 0.1% (v/v) Triton X-100 for 5 min. The cells were washed twice with PBS, 0.05 % (v/v) Tween-20 (PBS-Tween) and blocked with 1% (w/v) BSA in PBS for 30 min. The anti-Vinculin mouse antibody (1 mg ml^{-1} stock) (EMD Milipore Corp., USA) was applied at a 1:1000 v/v dilution for 1 h, then washed four times with PBS-Tween for 5 min, and an additional wash with 1% (w/v) BSA in PBS for 5 min. The secondary Alexa Fluor 488 goat anti-mouse antibody (2 mg ml^{-1} stock) and the TRITC-conjugated Phalloidin (0.06 mg ml^{-1}) (EMD Millipore Corp., USA) were both applied at a 1:1000 dilution (v/v) in 1% (w/v) BSA in PBS for 1 h. These were washed twice with PBS-Tween, incubated with 1:1000 DAPI (0.1 mg ml^{-1}) (EMD Milipore Corp., USA) in 1% (w/v) BSA in PBS for 5 min and washed with PBS-Tween. The stained cells were kept in PBS-Tween to prevent drying out.

Total Internal Reflection Fluorescence Microscopy: The focal adhesions-stained cells on the patterned glass coverslip substrates as those in 8-well μ -slides (ibiTreat, ibidi GmbH, Germany) were imaged using a Leica DMI8 Infinity TIRF microscope (Leica, Germany) with a 100x objective. After TRIF angle calibration, images were taken with automatic TIRF configuration setting, with adjustment of the penetration depth for optimal illumination and azimuth using LASX software (v.3.6). Lasers at 405, 488 and 561 nm were used to visualize fluorescence staining of nuclei (DAPI, emission: 435–485 nm), vinculin (primary anti-vinculin mouse and secondary Alexa Fluor 488 goat anti-mouse antibody, emission: 493–547 nm) and actin (TRITC Phalloidin, emission: 566–707 nm).

Statistical Analysis: If not indicated otherwise, the experimental data were evaluated using the arithmetic mean and standard deviation of triplicates. Comparison of multiple sample groups was statistically assessed with an one-way ANOVA test using the data analysis function in the software Excel (Microsoft Corporation, USA). Data were considered statistically significant if $p \leq 0.05$.

Supporting Information

Supporting Information is available from the Wiley Online Library or from the author.

Acknowledgements

This work was financially supported by the Bavarian-Czech Academic Agency, BTHA Grant No. JC-2019-21. The authors thank Prof. Thomas Scheibel, Chairholder of the Department of Biomaterials, University Bayreuth, for providing the facility to conduct this research, and Ing. Antonín Minařík (Centre of Polymer Systems, Tomas Bata University in Zlín, Czech Republic) for help with the profilometry measurements.

Open access funding enabled and organized by Projekt DEAL.

Conflict of Interest

The authors declare no conflict of interest.

Data Availability Statement

The data that support the findings of this study are available from the corresponding author upon reasonable request.

Keywords

aptamers, cancer cells, micropattern, nanofibrils, nanohydrogels, patterning, photolithography

Received: June 26, 2022

Revised: August 5, 2022

Published online: August 28, 2022

- [1] W. Hamilton, *Br. J. Gen. Pract.* **2010**, *60*, 121.
- [2] B. Hayes, C. Murphy, A. Crawley, R. O'Kennedy, *Diagnostics* **2018**, *8*, 39.
- [3] a) R. Vaidyanathan, R. H. Soon, P. Zhang, K. Jiang, C. T. Lim, *Lab Chip* **2018**, *19*, 11; b) W. Zhang, *J. Cancer Metastasis Treat.* **2021**, *7*, 22.
- [4] B. J. Green, T. Saberi Safaei, A. Mephram, M. Labib, R. M. Mohamadi, S. O. Kelley, *Angew. Chemi* **2016**, *55*, 1252.
- [5] Z. Shen, A. Wu, X. Chen, *Chem. Soc. Rev.* **2017**, *46*, 2038.
- [6] A. D. Hartkopf, P. Wagner, D. Wallwiener, T. Fehm, R. Rothmund, *Anticancer Res.* **2011**, *31*, 979.
- [7] a) C.-Y. Wu, C.-L. Lee, C.-F. Wu, J.-Y. Fu, C.-T. Yang, C.-T. Wen, Y.-H. Liu, H.-P. Liu, J. C.-H. Hsieh, *Diagnostics* **2020**, *10*, 144; b) F. Castro-Giner, N. Aceto, *Genome Med.* **2020**, *12*, 31.
- [8] a) M. Gijs, G. Penner, G. B. Blackler, N. R. E. N. Impens, S. Baatout, A. Luxen, A. M. Aerts, *Pharmaceuticals* **2016**, *9*, 29; b) W. Alshaer, N. Ababneh, M. Hatmal, H. Izmirlı, M. Choukeife, A. Shraim, N. Sharar, A. Abu-Shiekah, F. Odeh, A. Al Bawab, A. Awidi, S. Ismail, *PLoS One* **2017**, *12*, 0189558; c) M. J. Adler, D. S. Dimitrov, *Hematol. Oncol. Clin. North Am.* **2012**, *26*, 447.
- [9] M. Liu, W. Ma, Q. Li, D. Zhao, X. Shao, Q. Huang, L. Hao, Y. Lin, *Cell Proliferation* **2019**, *52*, 12511.
- [10] M. S. Nabavinia, A. Gholoobi, F. Charbgoon, M. Nabavinia, M. Ramezani, K. Abnous, *Med. Res. Rev.* **2017**, *37*, 1518.
- [11] J. Carvalho, A. Paiva, M. P. Cabral Campello, A. Paulo, J.-L. Mergny, G. F. Salgado, J. A. Queiroz, C. Cruz, *Sci. Rep.* **2019**, *9*, 7945.
- [12] W.-S. Shin, J. Gim, S. Won, S.-T. Lee, *Sci. Rep.* **2018**, *8*, 8519.
- [13] L. Chen, C. Yan, Z. Zheng, *Mater. Today* **2018**, *21*, 38.
- [14] S. Larrucea, C. González-Rubio, R. Cambroner, B. Ballou, P. Bonay, E. López-Granados, P. Bouvet, G. Fontán, M. Fresno, M. López-Trascasa, *J. Biol. Chem.* **1998**, *273*, 31718.
- [15] a) Z. Zhang, N. Chen, S. Li, M. R. Battig, Y. Wang, *J. Am. Chem. Soc.* **2012**, *134*, 15716; b) J. Sekine, S.-C. Luo, S. Wang, B. Zhu, H.-R. Tseng, H.-H. Yu, *Adv. Mater.* **2011**, *23*, 4788; c) S. Wang, K. Liu, J. Liu, Z. T.-F. Yu, X. Xu, L. Zhao, T. Lee, E. K. Lee, J. Reiss, Y.-K. Lee, L. W. K. Chung, J. Huang, M. Rettig, D. Seligson, K. N. Duraiswamy, C. K.-F. Shen, H.-R. Tseng, *Angew. Chem.* **2011**, *50*, 3084.
- [16] a) Q. Wei, T. Becherer, S. Angioletti-Uberti, J. Dzubiella, C. Wischke, A. T. Neffe, A. Lendlein, M. Ballauff, R. Haag, *Angew. Chem.* **2014**, *53*, 8004; b) S. Chen, L. Li, C. Zhao, J. Zheng, *Polymer* **2010**, *51*, 5283.
- [17] a) J. R. Clegg, N. A. Peppas, *Soft Matter* **2020**, *16*, 856; b) L. Abune, B. Davis, Y. Wang, *Wiley Interdiscip. Rev.: Nanomed. Nanobiotechnol.* **2021**, *13*, 1731.
- [18] T. B. Aigner, E. DeSimone, T. Scheibel, *Adv. Mater.* **2018**, *30*, 1704636.
- [19] M. Humenik, A. M. Smith, S. Arndt, T. Scheibel, *J. Struct. Biol.* **2015**, *197*, 130.
- [20] M. Humenik, M. Magdeburg, T. Scheibel, *J. Struct. Biol.* **2014**, *186*, 431.

- [21] A. Molina, T. Scheibel, M. Humenik, *Biomacromolecules* **2019**, *20*, 347.
- [22] M. Humenik, T. Preiß, S. Gödrich, G. Papastavrou, T. Scheibel, *Mater. Today. Bio.* **2020**, *6*, 100045.
- [23] C. Heinritz, Z. Lamberger, K. Kocourková, A. Minařík, M. Humenik, *ACS Nano* **2022**, *16*, 7626.
- [24] X. Chen, D. M. Kube, M. J. Cooper, P. B. Davis, *Mol. Ther.* **2008**, *16*, 333.
- [25] a) C. Brignole, V. Bensa, N. A. Fonseca, G. Del Zotto, S. Bruno, A. F. Cruz, F. Malaguti, B. Carlini, F. Morandi, E. Calarco, P. Perri, V. Moura, L. Emionite, M. Cilli, F. De Leonardis, A. Tondo, L. Amoroso, M. Conte, A. Garaventa, A. R. Sementa, M. V. Corrias, M. Ponzoni, J. N. Moreira, F. Pastorino, *J. Exp. Clin. Cancer Res.* **2021**, *40*, 180; b) G. R. Moe, L. M. Steirer, J. A. Lee, A. Shivakumar, A. D. Bolanos, *J. Exp. Clin. Cancer Res.* **2021**, *40*, 293.
- [26] D. Shangquan, Y. Li, Z. Tang, Z. C. Cao, H. W. Chen, P. Mallikaratchy, K. Sefah, C. J. Yang, W. Tan, *Proc. Natl. Acad. Sci. USA* **2006**, *103*, 11838.
- [27] L. Babelová, M. E. Sohová, A. Poturnayová, M. Buríková, J. Bizík, T. Hianik, *Electroanalysis* **2018**, *30*, 1487.
- [28] H. Zhang, Y. Ma, Y. Xie, Y. An, Y. Huang, Z. Zhu, C. J. Yang, *Sci. Rep.* **2015**, *5*, 10099.
- [29] A. Sadanand, V. Maximov, J. Lee, S. Suttapitugsakul, J. Shim, C. Doering, R. Wu, R. Schnepf, T. Spencer, K. Goldsmith, *Cancer Res.* **2021**, *81*, 3034.
- [30] P. J. Bates, D. A. Laber, D. M. Miller, S. D. Thomas, J. O. Trent, *Exp. Mol. Pathol.* **2009**, *86*, 151.
- [31] M. R. Karver, R. Weissleder, S. A. Hilderbrand, *Angew. Chem.* **2012**, *51*, 920.
- [32] M. Humenik, M. Drechsler, T. Scheibel, *Nano Lett.* **2014**, *14*, 3999.
- [33] S. I. Rudnick, G. P. Adams, *Cancer Biother. Radiopharm.* **2009**, *24*, 155.
- [34] a) A. Lopresti, F. Malergue, F. Bertucci, M. L. Liberatoscioli, S. Garnier, Q. DaCosta, P. Finetti, M. Gilibert, J. L. Raoul, D. Birnbaum, C. Acquaviva, E. Mamessier, *JCI Insight* **2019**, *5*, e128180. b) C. Sun, Y.-P. Hsieh, S. Ma, S. Geng, Z. Cao, L. Li, C. Lu, *Sci. Rep.* **2017**, *7*, 40632; c) S. L. Sahoo, C.-H. Liu, W.-C. Wu, *RSC Adv.* **2017**, *7*, 22468.
- [35] N. Malhotra, J.-S. Lee, R. A. D. Liman, J. M. S. Ruallo, O. B. Villaflores, T.-R. Ger, C.-D. Hsiao, *Molecules* **2020**, *25*, 3159.
- [36] T. U. Esser, V. T. Trossmann, S. Lentz, F. B. Engel, T. Scheibel, *Mater. Today Bio* **2021**, *11*, 100114.
- [37] S. Wohlrab, S. Müller, A. Schmidt, S. Neubauer, H. Kessler, A. Leal-Egaña, T. Scheibel, *Biomaterials* **2012**, *33*, 6650.
- [38] K. Schacht, T. Jüngst, M. Schweinlin, A. E. , J. Groll, T. Scheibel, *Angew. Chem. Int. Ed. Engl.* **2015**, *127*, 2858.
- [39] A. Lechner, V. T. Trossmann, T. Scheibel, *Macromol. Biosci.* **2022**, *22*, 2100390.
- [40] a) M. M. Dailey, M. C. Miller, P. J. Bates, A. N. Lane, J. O. Trent, *Nucleic Acids Res.* **2010**, *38*, 4877; b) A. Miranda, T. Santos, E. Largy, C. Cruz, *Pharmaceuticals* **2021**, *14*, 121; c) T. Santos, J. Lopes-Nunes, D. Alexandre, A. Miranda, J. Figueiredo, M. S. Silva, J.-L. Mergny, C. Cruz, *Biochimie* **2022**, *200*, 8.
- [41] J. Pei, H. Hall, N. D. Spencer, *Biomaterials* **2011**, *32*, 8968.
- [42] H. M. Herold, A. Döbl, S. Wohlrab, M. Humenik, T. Scheibel, *Biomacromolecules* **2020**, *21*, 4904.
- [43] M. E. Berginski, E. A. Vitriol, K. M. Hahn, S. M. Gomez, *PLoS One* **2011**, *6*, 22025.
- [44] J. D. Humphries, P. Wang, C. Streuli, B. Geiger, M. J. Humphries, C. Ballestrem, *J. Cell Biol.* **2007**, *179*, 1043.
- [45] N. Bodenberger, D. Kubiczek, L. Trösch, A. Gawanbacht, S. Wilhelm, D. Tielker, F. Rosenau, *Sci. Rep.* **2017**, *7*, 6151.
- [46] a) J. Nicolas, S. Magli, L. Rabbachin, S. Sampaolesi, F. Nicotra, L. Russo, *Biomacromolecules* **2020**, *21*, 1968; b) J. M. Muncie, V. M. Weaver, *Current Topics in Developmental Biology*, Vol. 130, (Eds: E. S. Litscher, P. M. Wassarman), Academic Press **2018**, p. 1.
- [47] a) J. Winkler, A. Abisoye-Ogunniyan, K. J. Metcalf, Z. Werb, *Nat. Commun.* **2020**, *11*, 5120; b) T. R. Cox, *Nat. Rev. Cancer* **2021**, *21*, 217.
- [48] S. Bonde, T. Berthing, M. H. Madsen, T. K. Andersen, N. Buch-Månson, L. Guo, X. Li, F. Badique, K. Anselme, J. Nygård, K. L. Martinez, *ACS Appl. Mater. Interfaces* **2013**, *5*, 10510.
- [49] S. Müller-Herrmann, T. Scheibel, *ACS Biomater. Sci. Eng.* **2015**, *1*, 247.
- [50] D. Steiner, S. Winkler, S. Heltmann-Meyer, V. T. Trossmann, T. Fey, T. Scheibel, R. E. Horch, A. Arkudas, *Biofabrication* **2021**, *13*, 045003.
- [51] a) M. Humenik, M. Mohrand, T. Scheibel, *Bioconjugate Chem.* **2018**, *29*, 898; b) M. B. Elsner, H. M. Herold, S. Müller-Herrmann, H. Bargel, T. Scheibel, *Biomater. Sci.* **2015**, *3*, 543.
- [52] M. Humenik, T. Scheibel, *ACS Nano* **2014**, *8*, 1342.
- [53] J. W. Nichol, S. T. Koshy, H. Bae, C. M. Hwang, S. Yamanlar, A. Khademhosseini, *Biomaterials* **2010**, *31*, 5536.
- [54] A. Agarwal, Y. Farouz, A. P. Nesmith, L. F. Deravi, M. L. McCain, K. K. Parker, *Adv. Funct. Mater.* **2013**, *23*, 3738.
- [55] B. G. Munoz-Robles, I. Kopyeva, C. A. DeForest, *Adv. Mater. Interfaces* **2020**, *7*, 2001198.
- [56] a) K. Kolostova, R. Matkowski, R. Gürlich, K. Grabowski, K. Soter, R. Lischke, J. Schützner, V. Bobek, *Cytotechnology* **2016**, *68*, 1095; b) Z.-P. Wang, M. A. Eisenberger, M. A. Carducci, A. W. Partin, H. I. Scher, P. O. P. Ts'o, *Cancer* **2000**, *88*, 2787; c) B. L. Khoo, S. C. Lee, P. Kumar, T. Z. Tan, M. E. Warkiani, S. G. W. Ow, S. Nandi, C. T. Lim, J. P. Thiery, *Oncotarget* **2015**, *6*, 15578; d) A. S. Berghoff, Y. Liao, M. A. Karreman, A. Ilhan-Mutlu, K. Gunkel, M. R. Sprick, C. Eisen, T. Kessler, M. Osswald, S. Wünsche, M. Feinauer, B. Gril, F. Marmé, L. L. Michel, Z. B. Horvath, F. Sahn, N. Becker, M. O. Breckwoldt, G. Solecki, M. Gömmel, L. Huang, P. Rübmann, C. M. Thome, M. Ratliff, A. Trumpp, P. S. Steeg, M. Preusser, W. Wick, F. Winkler, *Mol. Cancer Res.* **2021**, *19*, 688.
- [57] a) M.-Y. Kim, T. Oskarsson, S. Acharyya, D. X. Nguyen, X. H.-F. Zhang, L. Norton, J. Massagué, *Cell* **2009**, *139*, 1315; b) A. M. C. Barradas, L. W. M. M. Terstappen, *Cancers* **2013**, *5*, 1619; c) J. S. de Bono, H. I. Scher, R. B. Montgomery, C. Parker, M. C. Miller, H. Tissing, G. V. Doyle, L. W. W. M. Terstappen, K. J. Pienta, D. Raghavan, *Clin. Cancer Res.* **2008**, *14*, 6302.
- [58] R. Tudoreanu, I. M. Handrea-Dragan, S. Boca, I. Botiz, *Int. J. Mol. Sci.* **2022**, *23*, 7731.
- [59] A. Miranda, L. Martínez, P. A. A. de Beule, *MethodsX* **2020**, *7*, 100931.